

Locked Multichannel Generation and Management by Use of a Fabry–Perot Etalon in a Mode-Locked Cr:Forsterite Laser Cavity

Tzu-Ming Liu, Hsu-Hao Chang, Shi-Wei Chu, and Chi-Kuang Sun, *Senior Member, IEEE*

Abstract—We demonstrate a method to manage the locked multichannel output from a mode-locked Cr:forsterite laser cavity, which was achieved by inserting a Fabry–Perot etalon into the oscillator. It is found that the thickness of the etalon determines the channel spacing and its surface reflectivity affects channel linewidth and channel pulsewidth. Following Fabry–Perot theory, we can use these facts to control the characteristics of these locked multichannels.

Index Terms—Cr:forsterite, Fabry–Perot etalon, modelocking, multichannel, solid-state laser.

I. INTRODUCTION

FOR optical communications and signal processing, wavelength-division multiplexed (WDM) and optical time-division multiplexed (OTDM) formats are two commonly employed architectures. Recently, hybrid WDM/OTDM approaches have been proposed to exploit communication resources in both time and frequency domains. This novel photonic network requires multiple channels (with different wavelengths) of ultrashort and highly synchronized pulses. To date, most approaches realize multichannel operation by using semiconductor lasers, either in arrays of independent gain media [1], [2] or with a frequency control system of a single gain medium [3]–[5]. All of them require precise wavelength controllers, as well as an independent gain medium, for each channel [1], [2] or with complexity in output coupler management [5]. Besides, to realize a WDM/OTDM hybrid communication system, not only multiple channels but also mode-locked pulses are required. Therefore, it is necessary to have multiwavelength generation directly from a mode-locked laser oscillator. Shi *et al.* used a single stripe GaAs–AlGaAs semiconductor optical amplifier (SOA) to generate four wavelengths simultaneously with 0.3-mW channel power and 12-ps optical pulsewidth for each channel [6]. To operate around a 1.5- μm optical communication band, Papakyriakopoulos *et al.* employed an InGaAsP–InP ridge waveguide SOA and a Fabry–Perot filter in the cavity to produce ten channels of 20-ps pulses with 40- μW total power [7]. With a similar scheme, Vlachos *et al.* obtained the same channel number and shorter

7-ps pulses with a higher output power of 580 μW [8]. These actively mode-locked multiwavelength lasers not only preserve the advantage of relative wavelength stability between all oscillating modes but also result in a simpler experimental configuration. However, all of these multiwavelength mode-locked lasers can only achieve relatively low output power, on the order of several tens of microwatts, up to 1 mW [6]–[8]. In order to improve the output power level and increase the number of channels for telecommunication applications, it is essential to develop multiwavelength solid-state laser technologies based on high-power broadband laser crystals [9], [10] to provide multichannel operation. With these requirements, the mode-locked Cr:forsterite laser, whose operating wavelength can cover the communication band, is a suitable candidate. Seminal work to develop and advance Cr:forsterite lasers was made by Petrićević *et al.* at the City College of New York [11]–[13]. Recently, Chudoba *et al.* generated 14-fs pulses from a solid-state Cr:forsterite laser cavity with a spectrum covering the whole 1.3–1.55- μm communication band [14]. With a high output power, it is desirable to demonstrate a multichannel mode-locked solid-state laser based on Cr:forsterite laser crystals. This was recently achieved [15] by inserting a 0.15-mm cover glass, which serves as an etalon, into a Cr:forsterite laser cavity. Twelve phase-locked channels, each having 6–19-ps pulse width, have been generated around 1230 nm with 280 mW of average output power from a single laser oscillator. Along with generation, the management of parameters such as free spectral range (FSR), channel bandwidth, and channel pulsewidth are also required to distribute communication resources in a hybrid WDM/OTDM communications system. In this report, we study the effect of an etalon on managing the properties of these generated channels. Their characteristics were investigated with an autocorrelator and an SHG-based frequency resolved optical gating (FROG) technique [16]. Channel spacing, channel bandwidth, and channel pulsewidth were all found to be managed well with the inserted etalon.

II. EXPERIMENTAL SETUP

The structure of the laser resonator is shown schematically in Fig. 1. The laser constructed for this study used a 19-mm-long Brewster-cut Cr:forsterite crystal with a chromium (IV) ion concentration of $5 \times 10^{18} \text{ cm}^{-3}$. The crystal was oriented with its *b* axis in the horizontal plane, resulting in horizontal laser polarization. The laser was pumped with 8.5 W of 1064-nm

Manuscript received October 23, 2001; revised February 6, 2002. This work was supported by the National Science Council of Taiwan, R.O.C., under Grant 90-2215-E-002-039.

The authors are with the Department of Electrical Engineering and Graduate Institute of Electro-Optical Engineering, National Taiwan University, Taipei 10617, Taiwan, R.O.C. (e-mail: sun@cc.ee.ntu.edu.tw).

Publisher Item Identifier S 0018-9197(02)04111-8.

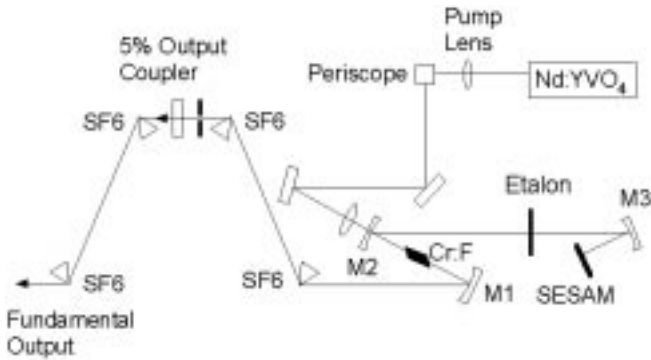


Fig. 1. Schematic diagram for the experimental setup.

light from a diode-pumped Nd:YVO₄ laser.¹ The Cr:forsterite crystal absorbed 75% of the 1064-nm pump, corresponding to an absorption coefficient $\alpha \sim 0.73 \text{ cm}^{-1}$. The crystal temperature was kept around 2 °C and a nitrogen purge prevented water condensation. A lens was placed at the pump-laser output to adjust the size of the pumping laser beam. Its polarization was rotated by using a periscope. A 10-cm lens was used to focus the pump beam through the cavity mirror M2 onto the Cr:forsterite crystal. The laser cavity had a folded configuration with a 5% output coupler, three laser mirrors (M1, M2, M3), and a semiconductor saturable absorber mirror (SESAM). The SESAM initiated and stabilized the femtosecond pulse generation. This technique has previously been applied to mode-locked Cr:forsterite lasers [17], [18], and optical pulses as short as 20 fs have been obtained [19]. In our study, the SESAM consisted of 25 periods of GaAs–AlAs quarter-wave layers, followed by an Al_{0.48}In_{0.52}As quarter-wave layer with two embedded Ga_{0.47}In_{0.53}As quantum wells. To provide the saturable absorber nonlinearity for initiating and stabilizing the Cr:forsterite laser, the quantum-well structure was designed to have the heavy-hole excitonic resonance around 1232 nm at room temperature. This resonant excitonic wavelength limited our laser operation wavelength to be around 1230 nm. The insertion loss of the SESAM was 2.5% with a saturation energy fluence of $\sim 50 \mu\text{J}/\text{cm}^2$. Mirrors M1 and M2 had a 10-cm radius of curvature, and mirror M3 had 20-cm radius of curvature. All mirrors were highly reflecting ($>99\%$) over the spectral range of the fundamental output (1200–1270 nm). An SF6 prism pair was inserted on the side of the cavity opposite the SESAM to provide compensation for intracavity group-velocity dispersion. A slit was placed before the output coupler to tune the lasing wavelength. Outside the cavity, we used another SF6 prism pair to achieve both beam shaping and dispersion compensation of the laser output. The etalon used in the cavity was a 0.15-mm cover glass² with a refractive index of 1.5, and was mounted upon a rotary stage to provide control of the incident angle. We used an optical spectrum analyzer (OSA) (Anritsu MS9710B) with a 0.07-nm spectral resolution to monitor the spectrum. To acquire data over an adequate spectral span with a limited number of sampling points, the spectral resolution of the OSA was set at 0.12 nm. A fiber

¹Spectra-Physics Millennia IR.

²Matsunami Glass.

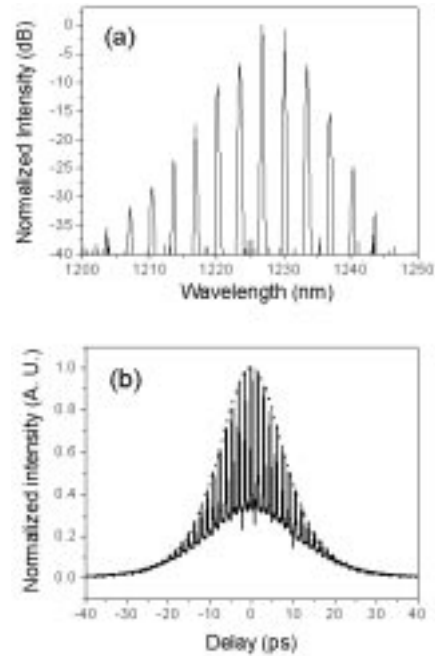


Fig. 2. (a) Output spectrum and (b) its corresponding autocorrelation trace of the multiwavelength Cr:forsterite laser output when the cover glass was inserted normal to the laser beam. Dotted line in (b) is a sech^2 fitting.

collimation lens with a 7.5-cm focal length was employed to couple the laser beam into the connector of a single mode fiber, which was connected to the OSA. We used a beam splitter after the external prism pair to direct a portion of the output to an autocorrelator. We also used this beam to make SHG FROG measurements with a 300- μm -thick β -barium borate crystal and a computer controlled stepping motor with 1- μm step size. The FROG signal was recorded by a CCD-based (Andor Technology DV420-OE) monochromator (Acton Research SP150) with a 1200-lines/mm grating. The spectrometer used in the FROG measurement has a 0.5-nm spectral resolution.

III. RESULTS AND DISCUSSIONS

A. Multichannel Generation

Without the etalon, the Cr:forsterite laser generated 130-fs pulses (assuming a sech^2 profile) at 81 MHz. The full-width half-maximum (FWHM) of the output spectrum was 13 nm, which resulted in a 0.334 time bandwidth product. After insertion of the etalon, simultaneous multichannel generation from the laser cavity was observed in the OSA. With the etalon at normal incidence, the output power was 280 mW. The corresponding spectrum is shown in Fig. 2(a) on a log scale. Twelve channels with a 0.2-nm channel bandwidth and a 3.36-nm FSR were observed. The average optical power of each channel ranged from 0.13 to 100 mW, which is sufficient for communication applications. With a sech^2 fit, the peak envelope of the spectrum has a 6.5-nm FWHM near 1227 nm. The corresponding autocorrelation trace [Fig. 2(b)] showed dense modulation over an envelope of 18.5-ps FWHM (Fig. 2(b), dotted curve). The spacing between each modulation peak was 1.52 ps and the modulation peak width, which was estimated by the FWHM of its peak-to-valley value, was around 266 fs.

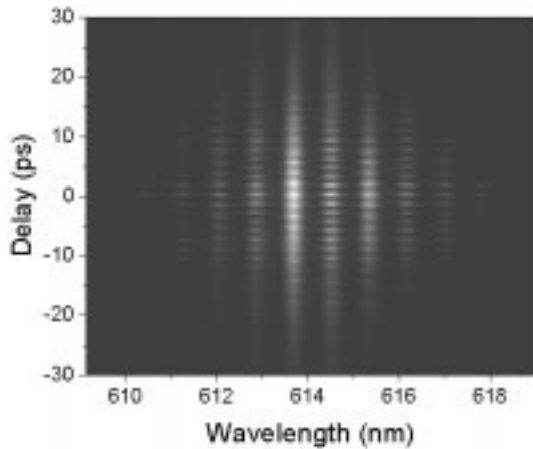


Fig. 3. SHG FROG trace of the multichannel Cr:forsterite laser output when the cover glass was inserted normal to the laser beam.

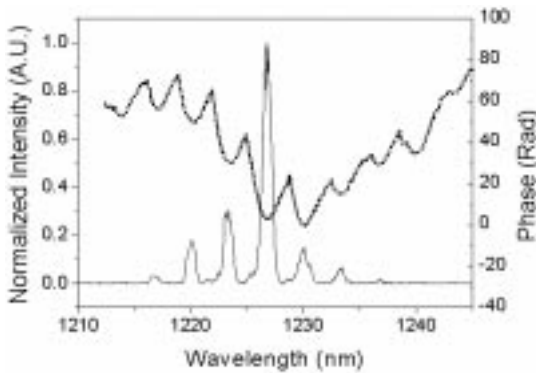


Fig. 4. Recovered intensity (solid curve) and phase (dotted curve) spectra from Fig. 3.

We have performed SHG FROG to further investigate the phase relation between different channels and to measure the optical pulsewidth of each channel. Fig. 3 illustrates the measured FROG trace with a linear scale, showing both temporal and spectral modulation. The signal at wavelengths 602.5–612 nm and 617–622.5 nm (second harmonic generation of the laser output) can only be observed easily in a log scale, in agreement with the measured spectrum, and is not visible in Fig. 3 because of dynamic range limitations. Fig. 4 shows the FROG-retrieved intensity and phase of the laser spectrum (both in linear scale). Strong phase correlation between different channels is shown. A wider retrieval spectrum displayed strong dispersion for each channel as a result of the spectral resolution limitation in the SHG measurement and the retrieval uncertainty caused by measurement noises. Nevertheless, good agreement with the measured spectrum in peak position and magnitude relation (dotted curve, same as Fig. 2(a), but in linear scale) was observed. We used a Fourier transformation to investigate the characteristics of each channel. The channel pulsewidth ranged from 8 to 19 ps, calculated with the data obtained from the FROG measurements. Fig. 5 (solid curve) shows a typical recovered pulse with a 12-ps FWHM.

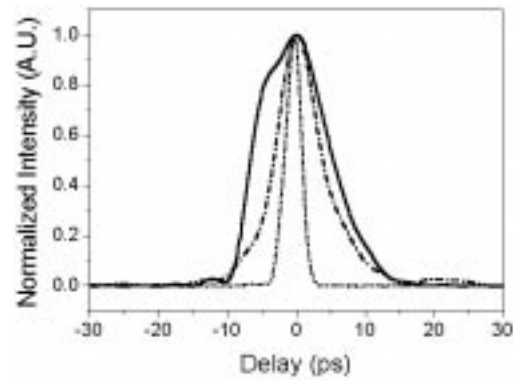


Fig. 5. Typical recovered channel pulse shape with 0° (solid curve), 30° (dashed-dotted curve), and 50° (dotted curve) incident angles of laser beam on the cover glass.

B. Multichannel Management

According to Fabry–Perot theory [20], the transmission spectrum of an etalon without loss shows modulation in wavelength domain and can be described by the formula

$$T = (1 - R)^2 / ((1 - R)^2 + 4R \sin^2(2\pi n d \cos \theta / \lambda)) \quad (1)$$

where

- R interface reflectivity between air and etalon;
- n refractive index of the etalon;
- d thickness of the etalon;
- θ refractive angle in the etalon;
- λ operating wavelength.

This spectrum can be characterized by two parameters. One is the wavelength spacing between each transmission peak, called the FSR, and it can be expressed as

$$\Delta\lambda = \lambda^2 / 2nd \cos \theta. \quad (2)$$

Obviously, the FSR will increase with decreasing thickness d and an increased incident angle on the etalon. The other is the depth of the modulation, which is defined as the ratio of the transmission maximum to the minimum value, and it can be derived as

$$V = (1 + R)^2 / (1 - R)^2. \quad (3)$$

According to electromagnetic wave theory, increasing the incident angle before the Brewster angle will decrease R , therefore reducing the spectral modulation depth and broadening the pass bandwidth of the etalon [21]. These facts imply that the channel spacing (free spectral range) and the channel pulsewidth can be manipulated by changing the etalon thickness d and the etalon interface reflectivity R , respectively. In order to investigate this, we changed the incident angle on the etalon, trying to control both the free spectral range and pass bandwidth, while the former determines the channel spacing and the latter determines the channel pulsewidth.

When tuning the incident angle between 0° and 50°, the same average output power was obtained. The measured spectra (in log scale) and their autocorrelation traces corresponding to two different incident angles, 30° and 50°, are shown in Figs. 6 and 7, respectively. With a larger incident angle, Fig. 6(a) shows a

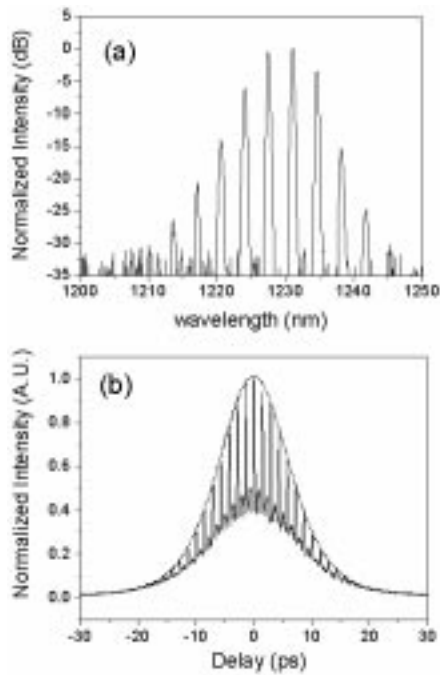


Fig. 6. (a) Output spectrum and (b) its corresponding autocorrelation trace of the multiwavelength Cr:forsterite laser output when the cover glass was turned 30° from normal incidence. Dotted line in (b) is a sech^2 fitting.

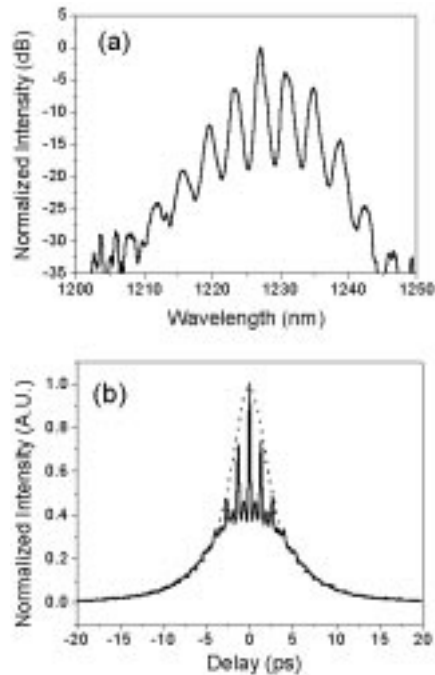


Fig. 7. (a) Output spectrum and (b) its corresponding autocorrelation trace of the multiwavelength Cr:forsterite laser output when the cover glass was turned 50° from normal incidence. Dotted line in (b) is a sech^2 fitting.

larger 3.48-nm FSR and a wider 0.24-nm channel bandwidth as compared with Fig. 2. Its corresponding autocorrelation trace [Fig. 6(b)] shows dense modulation over an envelope of 14.6-ps FWHM, assuming a sech^2 fit [Fig. 6(b), dotted curve]. The spacing between each modulation peak was 1.44 ps and the modulation peak-width was 213 fs, which agreed with

TABLE I
THEORETICAL AND EXPERIMENTAL VALUES OF FSR AND MODULATION SPACING FOR THE ETALON AT DIFFERENT INCIDENT ANGLES, 0° , 30° , AND 50°

Incidence angle	0°	30°	50°
Theoretical FSR	3.35 nm	3.55 nm	3.9 nm
Experimental FSR	3.36 nm	3.48 nm	3.96 nm
Theoretical modulation spacing	1.5 ps	1.41 ps	1.29 ps
Experimental modulation spacing	1.52 ps	1.44 ps	1.32 ps

the slightly wider 6.96-nm FWHM of the spectral envelope. When the angle was further turned to 50° , which is close to the Brewster angle (56°) of the etalon, the spectrum [Fig. 7(a)] shows an even larger FSR (3.96 nm) and an even wider channel bandwidth, which ranged from 0.84 to 1.56 nm. With a sech^2 fit, the corresponding autocorrelation trace shows even shorter 5.4-ps FWHM (Fig. 7(b), dotted curve) than previous cases. The corresponding modulation spacing was 1.32 ps, with a modulation peak-width of around 212 fs. The relatively fixed modulation peak-width corresponds to the relatively fixed spectral envelope observed when tuning the incident angle.

For channel spacing management, our experimental results agree well with the theoretical values at their corresponding incident angles (shown in Table I) with the following given parameters: $d = 0.15$ mm, $n = 1.5$, $\lambda = 1227$ nm, and $\theta =$ refractive angle in cover glass. Their errors are within the resolution of the spectrometer. From Fabry-Perot theory, the channel-spacing modulation-spacing product should be a constant (5.02 nm-ps) with the above parameters. The corresponding modulation spacings can then be calculated, and are very close to the observed experimental results. These excellent agreements between our observed behavior and Fabry-Perot theory, which is a frequency domain theory, imply that channel spacing can be designed via the thickness of the etalon.

To understand how interface reflectivity affects the channel pulsewidth, such as the normal-incidence case, we also performed SHG FROG with different incident angles. With the retrieved multichannel spectrum and its corresponding phase, the pulse shape in each individual channel can then be obtained. For the 30° case, the recovered channel pulsewidth ranged from 5.4 to 15.7 ps and Fig. 5 (dashed-dotted curve) shows a typical recovered pulse with a FWHM of 7 ps. For the 50° case, the recovered channel pulsewidth was reduced to 1.8–3.4 ps. Fig. 5 (dotted curve) also shows a typical recovered pulse-shape with 2.6-ps FWHM. Theoretical values of interface reflectivity R and modulation depth V are calculated and listed in Table II. With the surface reflectivity R decreased from 0.04 to 0.003, the measured channel bandwidth was increased from 0.2 to 1.56 nm, and the FWHM of the envelope from the autocorrelation trace decreased from 18.5 to 5.4 ps. At the same time, the channel pulsewidth was also reduced from 8–19 ps down to 1.8–3.4 ps (see Table II). The modulation depths of the laser spectra shown in Figs. 2, 6, and 7 share the same trend with the calculated

TABLE II
VALUES OF PARAMETERS, WHICH ARE RELATED TO INTERFACE
REFLECTIVITY, AT THREE DIFFERENT INCIDENT ANGLES, 0°, 30°, AND 50°

Incidence angle	0°	30°	50°
Interface reflectivity R	0.04	0.025	0.003
Modulation depth V	1.17	1.11	1.01
Channel linewidth	0.2 nm	0.24 nm	0.84–1.56 nm
Autocorrelation envelope width (FWHM)	18.5 ps	14.6 ps	5.4 ps
Channel pulse-width (FWHM)	8–19 ps	5.4–15.7 ps	1.8–3.4 ps

etalon value. These results indicate that manipulating the interface reflectivity R of the etalon can control the channel bandwidth, pulsewidth, and spectral modulation depth.

IV. SUMMARY

In conclusion, we have demonstrated spectral and temporal management of the output of a multiwavelength solid-state laser. Locked multiple channels were simultaneously generated from a mode-locked Cr:forsterite laser oscillator by inserting a cover glass as an etalon into the laser cavity. In agreement with Fabry–Perot theory, the channel spacing was tunable by changing the thickness of the etalon. The channel bandwidth, pulsewidth, and spectral modulation depth can all be simultaneously manipulated by changing the interface reflectivity of the etalon. With the recent broadband demonstration of Cr:forsterite lasers covering the whole telecommunication band from 1200 to 1580 nm, and the demonstration of high-repetition-rate passively mode-locked all-solid-state lasers [22], Cr:forsterite lasers show the potential for high-speed WDM/OTDM hybrid multiplexed communication systems when operated as high-power locked multichannel sources. Our study provides a simple method for generating and managing these evenly spaced multiple channels.

ACKNOWLEDGMENT

The authors would like to acknowledge the technical support by J.-K. Wang, L. A. Wang, and J.-Y. Lin.

REFERENCES

- [1] I. H. White, "A multichannel grating cavity laser for wavelength division multiplexing applications," *J. Lightwave Technol.*, vol. 9, pp. 893–889, July 1991.
- [2] M. C. Farries, A. C. Carter, G. C. Jones, and I. Bennion, "Tunable multiwavelength semiconductor laser with single fiber output," *Electron. Lett.*, vol. 27, pp. 1498–1499, Aug. 1991.
- [3] T. Hidaka and Y. Hatano, "Simultaneous two wavelength oscillation LD using biperiodic binary grating," *Electron. Lett.*, vol. 27, pp. 1075–1076, June 1991.
- [4] G. Coquin, K. Cheung, and M. M. Choy, "Single and multiple wavelength operation of acoustically tuned semiconductor lasers at 1.3 μm ," *IEEE J. Quantum Electron.*, vol. 25, pp. 1575–1579, June 1989.

- [5] N. Park, J. W. Dawson, and K. J. Vahala, "Multiple wavelength operation of an erbium-doped fiber laser," *IEEE Photon. Technol. Lett.*, vol. 4, pp. 540–541, June 1992.
- [6] H. Shi, J. Finlay, G. A. Alphonse, J. C. Connolly, and P. J. Delfyett, "Multiwavelength 10-GHz picosecond pulse generation from a single-stripe semiconductor diode laser," *IEEE Photon. Technol. Lett.*, vol. 9, pp. 1439–1441, Nov. 1997.
- [7] T. Papakyriakopoulos, A. Stavdas, E. N. Protonotarios, and H. Avramopoulos, "10 \times 10 GHz simultaneously modelocked multiwavelength fiber ring laser," *Electron. Lett.*, vol. 35, pp. 717–718, Apr. 1999.
- [8] K. Vlachos, K. Zoiros, T. Houbavlis, and H. Avramopoulos, "10 \times 30 GHz pulse train generation from semiconductor amplifier fiber ring laser," *IEEE Photon. Technol. Lett.*, vol. 12, pp. 25–27, Jan. 2000.
- [9] B. E. Bouma and J. G. Fujimoto, "Compact Kerr-lens mode-locked resonators," *Opt. Lett.*, vol. 21, pp. 134–136, Jan. 1996.
- [10] J. Aus der Au, G. J. Spühler, T. Südmeyer, R. Paschotta, R. Hövel, M. Moser, S. Erhard, M. Karszewski, A. Giesen, and U. Keller, "16.2-W average power from a diode-pumped femtosecond Yb:YAG thin disk laser," *Opt. Lett.*, vol. 25, pp. 859–861, June 2000.
- [11] V. Petričević, S. K. Gayen, R. R. Alfano, K. Yamagishi, H. Anzai, and Y. Yamaguchi, "Laser action in chromium-doped forsterite," *Appl. Phys. Lett.*, vol. 52, pp. 1040–1042, Mar 1988.
- [12] V. Petričević, S. K. Gayen, and R. R. Alfano, "Continuous-wave laser operation of chromium-doped forsterite," *Opt. Lett.*, vol. 14, pp. 612–614, June 1989.
- [13] A. Seas, V. Petričević, and R. R. Alfano, "Self-mode-locked chromium-doped forsterite laser generates 50-fs pulses," *Opt. Lett.*, vol. 18, pp. 891–893, June 1993.
- [14] C. Chudoba, J. G. Fujimoto, E. P. Ippen, H. A. Haus, U. Morgner, F. X. Kärtner, V. Scheurer, G. Angelow, and T. Tschudi, "All-solid-state Cr:forsterite laser generating 14-fs pulses at 1.3 μm ," *Opt. Lett.*, vol. 26, pp. 292–294, Mar 2001.
- [15] T. M. Liu, S. P. Tai, H. H. Chang, and C. K. Sun, "Simultaneous multiwavelength generation from a mode-locked all-solid-state Cr:forsterite laser," *Opt. Lett.*, vol. 26, pp. 834–836, June 2001.
- [16] K. W. DeLong, R. Trebino, J. Hunter, and W. E. White, "Frequency-resolved optical gating with the use of second-harmonic generation," *J. Opt. Soc. Amer. B*, vol. 11, pp. 2206–2215, Nov. 1994.
- [17] P. T. Guerreiro, S. Ten, E. Slobochikov, Y. M. Kim, J. C. Woo, and N. Peyghambarian, "Self-starting mode-locked Cr:forsterite laser with semiconductor saturable Bragg reflector," *Opt. Commun.*, vol. 136, pp. 27–30, Mar. 1997.
- [18] Z. Zhang, K. Torizuka, T. Itatani, K. Kobayashi, T. Sugaya, and T. Nakagawa, "Self-starting mode-locked femtosecond forsterite laser with a semiconductor saturable-absorber mirror," *Opt. Lett.*, vol. 22, pp. 1006–1008, July 1997.
- [19] Z. Zhang, K. Torizuka, T. Itatani, K. Kobayashi, T. Sugaya, T. Nakagawa, and H. Takahashi, "Broadband semiconductor saturable-absorber mirror for a self-starting mode-locked Cr:forsterite laser," *Opt. Lett.*, vol. 23, pp. 1465–1467, Sept. 1998.
- [20] H. A. Haus, *Waves and Fields in Optoelectronics*. Englewood Cliffs, NJ: Prentice-Hall, 1984, pp. 65–69.
- [21] ———, *Waves and Fields in Optoelectronics*. Englewood Cliffs, NJ: Prentice-Hall, 1984, pp. 35–36.
- [22] T. R. Schibli, T. Kremp, U. Morgner, F. X. Kärtner, R. Butendeich, J. Schwarz, H. Schweizer, F. Scholz, J. Hetzler, and M. Wegener, "Continuous-wave operation and Q -switched mode locking of Cr⁴⁺:YAG microchip lasers," *Opt. Lett.*, vol. 26, pp. 941–943, June 2001.



Tzu-Ming Liu was born in Keelung, Taiwan, R.O.C., in 1977. He received the B.S. degree in electrical engineering in 1999 from National Taiwan University, Taipei, R.O.C., where he is currently working toward the Ph.D. degree.

Since 1999, he has been with the Ultrafast Optics Group, Department of Electrical Engineering and Graduate Institute of Electro-Optical Engineering, National Taiwan University. His research interests include carrier dynamics in semiconductor materials, ultrafast solid-state lasers, multiphoton confocal microscopy, and nonlinear optics.

Hsu-Hao Chang was born in Taipei, Taiwan, R.O.C., in 1978. He received the B.S. degree in electrical engineering from National Taiwan University, Taipei, R.O.C., in 2000.

From 1999 to 2000, he took part in the research at the Ultrafast Optics Group, Department of Electrical Engineering and Graduate Institute of Electro-Optical Engineering, National Taiwan University.



Shi-Wei Chu was born in Taipei, Taiwan, R.O.C., in 1977. He received the B.S. degree in electrical engineering in 1999 and the M.S. degree in electrooptical engineering in 2001, both from National Taiwan University, Taipei, R.O.C., where he is currently working toward the Ph.D. degree.

Since 1999, he has been with the Ultrafast Optics Group, Department of Electrical Engineering and Graduate Institute of Electro-Optical Engineering, National Taiwan University. His research interests include multiphoton confocal microscopy and

nonlinear optics in semiconductor materials.



Chi-Kuang Sun (M'96-SM'01) was born in Tainan, Taiwan, R.O.C., in 1965. He received the B.S. degree in electrical engineering from National Taiwan University, Taipei, R.O.C., in 1987, and the M.S. and Ph.D. degrees in applied physics from Harvard University, Cambridge, MA, in 1990 and 1995, respectively.

He was a Visiting Scientist at the Research Laboratory of Electronics, Massachusetts Institute of Technology, Cambridge, MA, between 1992–1994, working on femtosecond carrier dynamic studies of semiconductors and metals. He was with the National Science Foundation Center of Quantized Electronics Structures (QUEST), University of California at Santa Barbara, from 1995 to 1996 as an Assistant Research Engineer, conducting research on quantum dots, GaN, microcavity, high-speed communication devices and systems. He is now an Associate Professor in the Graduate Institute of Electro-Optical Engineering and Department of Electrical Engineering, National Taiwan University. His research is primarily concerned with femtosecond laser technology, high-speed optoelectronic devices, ultrafast phenomena, novel quantum structures, GaN, and biomedical optics.

Dr. Sun is a member of the American Physical Society, the Optical Society of America (OSA), and the IEEE Laser and Electro-Optics Society (LEOS). He was the recipient of the 2000 C.N. Yang Outstanding Young Researcher Award from the Association of Asian Pacific Physical Society.